

PALM: Pushing Adaptive Learning Rate Mechanisms for Continual Test-Time Adaptation

Sarthak Kumar Maharana, Baoming Zhang, Yunhui Guo

The University of Texas at Dallas, Richardson, USA
 {sarthak.maharana, baoming.zhang, yunhui.guo}@utdallas.edu

Abstract

Real-world vision models in dynamic environments face rapid shifts in domain distributions, leading to decreased recognition performance. Using unlabeled test data, continual test-time adaptation (CTTA) directly adjusts a pre-trained source discriminative model to these changing domains. A highly effective CTTA method involves applying layer-wise adaptive learning rates for selectively adapting pre-trained layers. However, it suffers from the poor estimation of domain shift and the inaccuracies arising from the pseudo-labels. This work aims to overcome these limitations by identifying layers for adaptation via quantifying model prediction uncertainty without relying on pseudo-labels. We utilize the magnitude of gradients as a metric, calculated by back-propagating the KL divergence between the softmax output and a uniform distribution, to select layers for further adaptation. Subsequently, for the parameters exclusively belonging to these selected layers, with the remaining ones frozen, we evaluate their sensitivity to approximate the domain shift and adjust their learning rates accordingly. We conduct extensive image classification experiments on CIFAR-10C, CIFAR-100C, and ImageNet-C, demonstrating the superior efficacy of our method compared to prior approaches.

Code — <https://github.com/sarthaxxxx/PALM>

Introduction

In a real-world setting, machine-perception systems (Arnold et al. 2019) function in a rapidly changing environment. Pre-trained vision models are susceptible to performance degradation caused by potential distribution shifts in such contexts. For instance, while these models may have been trained on clean images, images captured by sensors could be corrupted by various weather conditions.

In the realm of addressing domain shifts due to image corruptions, *test-time adaptation* (TTA) has been gaining a lot of traction lately (Döbler, Marsden, and Yang 2023; Wang et al. 2020). Here, a pre-trained source model, with no access to its training (source) data due to privacy, is adapted to unlabeled test data through online training. One strategy in TTA involves mitigating domain shifts by adjusting the source model parameters using pseudo labels and minimizing the entropy of the model predictions (Wang et al. 2020).

Copyright © 2025, Association for the Advancement of Artificial Intelligence (www.aaai.org). All rights reserved.

While this approach effectively adapts the model to a single type of corruption, it faces two constraints when continually applied across a sequence of test tasks featuring different corruptions. Firstly, there is the issue of *error accumulation* since pseudo labels are generated for unlabeled test data, errors accumulate over time. Secondly, *catastrophic forgetting* occurs, resulting in a long-term loss of the model’s source knowledge due to adaptations and large parameter updates across tasks.

Continual test-time adaptation (CTTA) has been recently introduced to tackle these challenges. In (Niu et al. 2022; Gong et al. 2022; Wang et al. 2020; Schneider et al. 2020), stable optimization is achieved by updating the batch normalization (BN) parameters or re-formulating its statistics. CoTTA (Wang et al. 2022) includes full model updates, with a teacher-student network setup, to handle the above issues. To further improve the performance of CoTTA, EcoTTA (Song et al. 2023) introduces the attachment of “meta networks”, *i.e.*, a BN layer and a convolution block, to the frozen source model for efficient adaptation.

More recently, the authors in (Lee et al. 2022) demonstrated that based on the type of distributional shift of the test data, a certain subset of layers of a pre-trained model can be “surgically” or heuristically chosen to fine-tune. Inspired by this finding, *Layer-wise Auto-Weighting* (LAW) (Park et al. 2024) was introduced recently. LAW utilizes the Fisher Information Matrix (FIM) (Sagun et al. 2017) to estimate domain shifts, automatically weighting trainable parameters and adjusting their learning rates (LRs) accordingly. While LAW achieves state-of-the-art results for CTTA, it still encounters two significant limitations: **1)** It presupposes that layer-wise importance can be accurately estimated via FIM with initially generated pseudo-labels. Nevertheless, it is widely recognized that pseudo-labels are inherently noisy and unreliable. **2)** Relying on directly accumulating such approximated importance from noisy labels to calculate domain shifts can lead to inaccuracies.

In this paper, we present a novel method called **PALM** to push the limits of adaptive learning rate methods for CTTA. To address catastrophic forgetting, our approach begins by identifying a subset of layers that significantly contribute to the uncertainty of model predictions. Rather than relying on pseudo-labels, we determine layer-wise importance by leveraging information from the gradient space, specif-

ically by calculating the Kullback-Leibler (KL) divergence between the model output and a uniform distribution. This approach eliminates dependence on pseudo-labels and enables a more accurate estimation of layer-wise importance. Subsequently, the LRs of the parameters of these selected layers are adjusted based on the degree of domain shift observed in the test data. We use parameter sensitivity as an indicator of domain shift and employ weighted moving averages to aggregate sensitivity from previous test batches. Our approach provides a more accurate estimation of domain shift compared to existing adaptive LR methods, leading to more effective adjustments in LRs.

To summarise, our contributions are as follows: **1)** We present **PALM**, introducing novel improved schemes for CTTA with a specific focus on addressing the key limitations of existing adaptive learning rate methods. **2)** Considering the model’s *prediction uncertainty* at test-time, we automatically select and adapt layers requiring further updates while *freezing* the rest. We adjust learning rates based on *parameter sensitivity* to estimate domain shift, making the overall process *computationally inexpensive*. **3)** Our method delivers superior results, via extensive evaluations, in both *continual* and *gradual TTA* across three standard benchmark datasets.

Related Works

Test-time adaptation (TTA): The goal of TTA is to adapt source models to unlabelled test data in real-time using a source-free online approach (Jain and Learned-Miller 2011; Sun et al. 2020; Wang et al. 2020). TENT (Wang et al. 2020) optimizes BN parameters by minimizing the Shannon entropy (Shannon 1948) of pseudo labels. BN Stats Adapt (BN-1) (Schneider et al. 2020) replaces the BN statistics with those from corrupted test data, while AdaContrast (Chen et al. 2022) uses contrastive learning and a memory module to update the entire model. However, these methods address only single domain shifts and overlook continual shifts.

Continual TTA (CTTA): CTTA requires models to adapt to dynamic domain shifts. CoTTA (Wang et al. 2022) uses a teacher-student setup with full model updates. The teacher model is updated using an exponential moving average (EMA) to deal with catastrophic forgetting and error accumulation with time. EcoTTA (Song et al. 2023) adds “meta networks” to a frozen source model, computing an L_1 regularization loss to prevent catastrophic forgetting. DSS (Wang et al. 2024) introduces a dynamic thresholding framework to differentiate between low and high sample quality.

Efficient model fine-tuning: Freezing model parameters to learn information from downstream data has witnessed a good body of work (Sener et al. 2016; Long et al. 2016; Zintgraf et al. 2019; Guo et al. 2019). Depending upon the distribution shift of the target task, in (Lee et al. 2022), the authors demonstrate that heuristically selecting a subset of convolutional blocks for training while freezing the remaining blocks works better than full fine-tuning.

Adaptive LR methods: Research such as (Yosinski et al. 2014; Zeiler and Fergus 2014) demonstrates that deeper layers of a network extract task-specific features, unlike shallow

layers. AutoLR (Ro and Choi 2021) developed an adaptive LR scheme based on weight variations between layers, although these rates tend to mostly stay constant during training. For CTTA, LAW (Park et al. 2024) uses the FIM (Sagun et al. 2017) to assess domain shifts and adjust parameter LRs accordingly. However, using pseudo-labels to calculate FIM may lead to inaccuracies, and accumulating FIMs across domains can result in errors. Moreover, the adjustment of LR weights for each layer is constrained by the base LR, disregarding the relative “sensitivity” of parameters to the adaptation needs of the current batch and domain.

Parameter sensitivity: Neural network pruning literature extensively explores parameter sensitivity (LeCun, Denker, and Solla 1989; Luo, Wu, and Lin 2017; Theis et al. 2018; Molchanov et al. 2019). It suggests that less sensitive parameters require higher LRs for effective adaptation, and vice-versa. Additionally, (Liang et al. 2022) introduces a concept of temporal sensitivity variation, influenced by uncertainty, as a factor in training models for tasks like natural language understanding and machine translation.

Preliminary

Problem setup: CTTA aims to adapt a discriminative source model, parameterized as θ^s and trained on the source dataset $(\mathcal{X}^{\text{source}}, \mathcal{Y}^{\text{source}})$, to multiple incoming tasks $\mathcal{T}_i = \{x_k\}_{k=1}^K$, at test-time. Each \mathcal{T}_i signifies the i^{th} task with K batches, across varying data distributions. At time step $t=0$, the model is initialized to θ^s . It is then gradually adapted to each incoming batch x_k of \mathcal{T}_i in an **online** manner, where the model parameters are updated to θ^t . The source dataset is unavailable in this adaptation process due to privacy and storage constraints. With the continuum of tasks, at each t , the complete model parameters θ^t consist of a deep tensor with N layers, expressed as $\theta^t = \{\theta_1^t, \dots, \theta_N^t\}$. Each layer θ_n^t can be represented by $\theta_n^t = \{\theta_{1,n}^t, \dots, \theta_{j,n}^t, \dots\}$, where $\theta_{j,n}^t$ is an arbitrary parameter of layer θ_n^t .

Core motivations: We provide a detailed view of **surgical fine-tuning (SFT)** (Lee et al. 2022), **AutoLR** (Ro and Choi 2021), and **LAW** (Park et al. 2024). It is critical to understand the design principles and reasons for having an adaptive LR scheme for CTTA, which motivates this work.

To preserve the information during the source pre-training phase while fine-tuning on a target task of a different distribution like an image corruption, **SFT** empirically shows that heuristically fine-tuning only the first convolutional block results in better performance over full fine-tuning. Even though it is a desirable outcome for efficient fine-tuning, in this work, we close the gap by automatically selecting the layers that would adapt well to the target task.

Inspired by (Yosinski et al. 2014; Zeiler and Fergus 2014), **AutoLR**, proposed for supervised model fine-tuning on a downstream task, claims that the weight changes across layers should be in an increasing order, where the weight change δw_n in the n^{th} layer with weights w_n at training epoch e is $\delta w_n = \|w_n^e - w_n^{(e-1)}\|$. They hypothesize that initial layers, which extract general features, should have minimal δw_n , while deeper layers extract task-specific features. An adaptive LR optimization scheme constrains

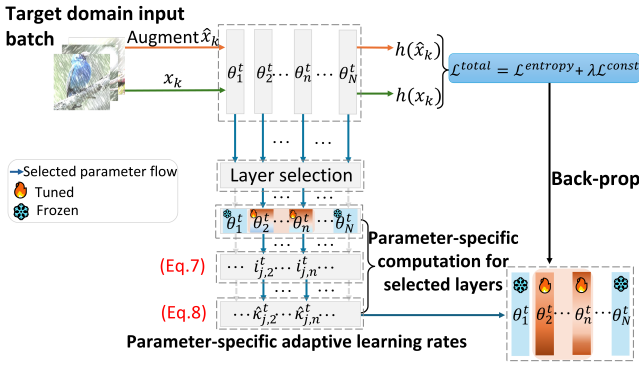


Figure 1: The framework of our proposed method *PALM*.

weight variations to increase across layers, without assessing each layer’s importance during adaptation. However, the LRs for each layer show minimal deviation and remain consistent throughout the training process.

As the first adaptive LR work for CTTA, **LAW** hypothesizes that identifying and controlling the adaptation rate of the different layers is useful (Lee et al. 2022). To understand the loss landscape and layer importance, the authors compute the gradient from the log-likelihood as $s(\theta_{j,n}^t; x_k) = \nabla_{\theta_{j,n}^t} \log(p(x_k))$, where $p(x_k)$ is the predicted output. Then, the FIM (Sagun et al. 2017), as a domain-shift indicator, is computed as a first-order approximation of the Hessian matrix. This layer-wise importance scheme completely relies on the pseudo-labels to compute the log-likelihood and is highly unreliable and uncertain. Due to the distribution shift, the label quality would begin to decrease for a continuum of tasks. The authors also propose to capture “domain-level” FIM (\hat{F}_n^t), for each layer, by a direct accumulation of the current layer-wise FIM (F_n^t) as, $\hat{F}_n^t = \hat{F}_n^{t-1} + F_n^t$.

This means that LAW puts equal emphasis on \hat{F}_n^t and F_n^t , for each layer. An issue arises when F_n^t of the current batch is small but gets outweighed by a “relatively” larger \hat{F}_n^t . This raises questions on the amount of adaptation required by the n^{th} layer for batch x_k as the FIMs dynamically change for each test batch. This leads to a possible imbalance between the accumulated FIMs \hat{F}_n^t and the current FIM F_n^t .

Drawing from these primary observations, our method focuses on addressing the following: **1)** Based on the prediction uncertainty of the model, we automatically select a subset of layers that would require further adaptation to a task, without relying on the pseudo-labels. **2)** As a domain shift indicator, we leverage the idea of parameter sensitivity of these layers only and adaptively alter their learning rates. We freeze the parameters of the unselected layers.

Proposed Methodology

Figure 1 illustrates our approach in **two** stages.

Layer selection by quantifying prediction uncertainty: CTTA maximizes model performance in the current domain and so it is vital to assess prediction certainty amidst rapid

domain shifts. In the literature on continual learning and TTA, several works utilize FIM (Kirkpatrick et al. 2017; Schwarz et al. 2018; Park et al. 2024). However, the unavailability of true labels, with unknown distribution, pushes us to capture the model prediction uncertainty and adapt selected layers, automatically chosen, to a batch of test data, unlike SFT (Lee et al. 2022).

Motivated by (Huang, Geng, and Li 2021), which proposed an uncertainty scoring function from the gradient space, we compute the gradients of each layer. In essence, we backpropagate the KL divergence between the softmax probabilities and a uniform distribution $\mathbf{u} = [\frac{1}{C}, \dots, \frac{1}{C}] \in \mathbb{R}^C$, where C is the total number of classes of the current task. This is a measurement of how far the distribution of the model’s prediction is from a uniform distribution. Intuitively, the KL divergence will be small with a large distribution shift. Let $h(\cdot)$ denote the classifier of the model. The loss $\mathcal{L}(\theta^t)$, to compute the gradients, is computed as follows,

$$\mathcal{L}(\theta^t) = \text{KL}(\text{softmax}(h(x_k)/T) || \mathbf{u}) \quad (1)$$

where the classifier’s output logits $h(x_k)$ is smoothed by a temperature T . Let $\hat{h}(x_k) = h(x_k)/T$. Our intuition is that since batches within the same task are of the same distribution, smoothing the logits with large values of T will make them indistinguishable. With model parameters θ^t , the gradients ($\nabla_{\theta_{j,n}^t} \mathcal{L}(\theta^t) = \frac{\partial \mathcal{L}(\theta^t)}{\partial \theta_{j,n}^t}$) can be simplified to,

$$\nabla_{\theta_{j,n}^t} \mathcal{L}(\theta^t) = \frac{1}{C} \sum_{c=1}^C \frac{\partial \mathcal{L}_{\text{CE}}(\hat{h}(x_k), c)}{\partial \theta_{j,n}^t} \quad (2)$$

Overall, the gradients boil down to the averaged cross-entropy loss between the smoothed output logits and a uniform label (Eq. 2). In CTTA, since ground-truth labels are absent, the gradients are more indicative of familiarity of the model with the batch of data. For batches within the same task, that share the same distribution, the vector norm of Eq. 2 would be higher because of a higher KL divergence since the softmax predictions would be less uniformly distributed. However, if the norm is smaller, this would mean that the softmax outputs are closer to \mathbf{u} . Our key idea is to select all the parameters of layers with the gradient norms to be less than or equal to a threshold η . *Layers with small gradient norms would require more adaptation for the model to make a confident prediction. We freeze the unselected layers which also helps to alleviate catastrophic forgetting to a large extent by preserving the prior source knowledge.* So, the scoring function, for each layer’s parameters, is defined as $\mathcal{Z}_{\theta_{j,n}^t} = \|\nabla_{\theta_{j,n}^t} \mathcal{L}(\theta^t)\|_1$. As mentioned earlier, $\mathcal{Z}_{\theta_{j,n}^t} \leq \eta$ allows the model to adaptively determine which specific layers need further adaptation. We freeze the layers with $\mathcal{Z}_{\theta_{j,n}^t} > \eta$ i.e., set their LR to 0.

Parameter sensitivity as a domain shift indicator: New studies have found that model parameters demonstrate levels of criticality (Zhang, Bengio, and Singer 2022) across different positions. Moreover, not all parameters adapt uniformly, and removing some can lower test generalization errors (Mozer and Smolensky 1988; Rasmussen and Ghahramani 2000). Inspired by this observation, we assert that pa-

rameters contribute differently during CTTA. From the previous stage, we automatically select the layers based on the prediction uncertainty. For parameters of these selected layers only, we compute their sensitivity *i.e.*, an approximation of an error when it is removed. Motivated by (Molchanov et al. 2016, 2019), we compute the sensitivity of a parameter $\theta_{j,n}^t$ based on the loss (Eq. 1) as follows,

$$S_{j,n}^t = \mathcal{L}(\theta^t) - \mathcal{L}(\theta^t | \theta_{j,n}^t = 0) \quad (3)$$

Precisely, $S_{j,n}^t$ approximates the change in the loss landscape at θ^t when $\theta_{j,n}^t$ is removed. Sensitivity, computed as a ‘‘weighting factor’’ of model weights (Molchanov et al. 2016, 2019; Liang et al. 2022), determines the level of adaptation needed for model parameters. We utilize the gradients of parameters from the selected layers, computed by Eq. 2, to compactly derive Eq. 3 from the first-order Taylor series expansion of $\mathcal{L}(\theta^t)$ (Lee, Ajanthan, and Torr 2018) to,

$$S_{j,n}^t = |\theta_{j,n}^t \nabla_{\theta_{j,n}^t} \mathcal{L}(\theta^t)| \quad (4)$$

Our rationale is as follows: parameters with low sensitivity are pushed to have higher LR’s owing to more adaptation. However, $S_{j,n}^t$ of $\theta_{j,n}^t$ can be highly uncertain and would have a large variation. We introduce a method to capture this ‘‘domain-level’’ uncertainty by computing a weighted moving average of the sensitivity $S_{j,n}^t$. This is formulated as,

$$\hat{S}_{j,n}^t = \alpha S_{j,n}^t + (1 - \alpha) \hat{S}_{j,n}^{(t-1)} \quad (5)$$

where $\hat{S}_{j,n}^t$ denotes the ‘‘domain-level’’ sensitivity, computed on-the-fly, and $\alpha \in [0,1]$ is a smoothing factor. Specifically, α decides the contribution of the current sensitivity $S_{j,n}^t$ to $\hat{S}_{j,n}^t$. Since CTTA happens at the batch level, it is critical to achieve a good balance between $S_{j,n}^t$ and $\hat{S}_{j,n}^t$, with a slightly larger focus on $S_{j,n}^t$. As can be seen, we do not directly accumulate the ‘‘domain-level’’ information, unlike LAW. Due to large distribution shifts happening because of the continuum of tasks, larger deviations of S_n^t from \hat{S}_n^t are bound to happen. We quantify this statistic as an absolute difference,

$$\hat{D}_{j,n}^t = |S_{j,n}^t - \hat{S}_{j,n}^t| \quad (6)$$

We emphasize that since Eq. 5 leverages sensitivity from previously computed batches and domains, $\hat{D}_{j,n}^t$ would act as a good indicator of how uncertain $S_{j,n}^t$ is to the previous batches and domains *i.e.* $\hat{S}_{j,n}^t$, for $\theta_{j,n}^t$. This would take care of error accumulation too. To automatically alter the LR’s of these parameters, the ‘‘importance’’ ($i_{j,n}^t$) is calculated as,

$$i_{j,n}^t = \hat{D}_{j,n}^t / \hat{S}_{j,n}^t \quad (7)$$

Eq. 6 enforces $\hat{D}_{j,n}^t \geq 0$ which, in turn, makes $i_{j,n}^t \geq 0$. And so, the final learning rate to update $\theta_{j,n}^t$ would be,

$$\hat{\kappa}_{j,n}^t = \kappa * i_{j,n}^t \quad (8)$$

where κ is the base fixed LR. The intuition behind the formulation of Eq. 7 is - smaller values of $\hat{S}_{j,n}^t$ indicate lower

sensitivity, and hence larger parameter updates are required via promoting the LR. At the same time, large uncertainties by $\hat{D}_{j,n}^t$ would also require larger updates. To avoid any overflow/underflow, we add ϵ ($0 < \epsilon \ll 1$) to the numerator and the denominator in Eq. 7.

Optimization: Though our method is robust, it is necessary to avoid miscalibrated labels. TENT (Wang et al. 2020) minimized the entropy on the output logits, l , following $\mathcal{H}(l) = -\sum_c p(l_c) \log(p(l_c))$, where $p(l_c)$ is the probability for class c . Following EcoTTA (Song et al. 2023), we use entropy minimization as the objective for adaptation where $\mathcal{H}(l)$ is minimized for samples below a certain fixed threshold \mathcal{H}_0 as,

$$\mathcal{L}^{entropy} = \mathbf{1}_{\mathcal{H}(l) \leq \mathcal{H}_0} \mathcal{H}(l) \quad (9)$$

\mathcal{H}_0 is set to $0.4 \times \log C$ following EcoTTA. For a fair comparison with prior works (Wang et al. 2022; Park et al. 2024), we apply a consistency loss between l and \hat{l} , computed as the output logits from the augmented version of x_k , to regularize the model as follows,

$$\mathcal{L}^{const} = -\sum_c p(l_c) \log(p(\hat{l}_c)) \quad (10)$$

where, $p(\hat{l}_c)$ is the probability for class c . Our overall optimization objective is as follows,

$$\mathcal{L}^{total} = \mathcal{L}^{entropy} + \lambda \mathcal{L}^{const} \quad (11)$$

where λ is a regularisation coefficient. In summary, upon calculating the parameter-specific LR’s (Eq. 8), we optimize the continually fine-tuned model to minimize Eq. 11.

Experiments and Results

We evaluate our proposed method in a CTTA setting, comparing it to state-of-the-art approaches, and extend our study to the gradual test-time adaptation (GTTA) setting following (Wang et al. 2022; Park et al. 2024).

Experimental Settings and Baselines

Datasets and Tasks: Following the standard benchmarks set by (Wang et al. 2022), we evaluate our proposed method on CIFAR-10C, CIFAR-100C, and ImageNet-C, based on image corruption schemes as set in (Hendrycks and Dietterich 2019). Each dataset contains a set of 15 corruption styles as tasks (*e.g.* gaussian noise, shot noise, . . .) with 5 severity levels. We follow CoTTA and apply the same test-time augmentations, like color jitter, gaussian blur, gaussian noise, random flips, and random affine, to the input x_k . As the evaluation metric, we report the mean classification error.

CTTA implementation details: To maintain fairness regarding the source models, we employ WideResNet-28 (36.4M params) (Zagoruyko and Komodakis 2016) for CIFAR-10C, ResNeXt-29 (6.8M params) (Xie et al. 2017) for CIFAR-100C, and ResNet-50 (23.5M params) (He et al. 2016) for ImageNet-C, all available on RobustBench (Croce et al. 2020). We optimize using an Adam optimizer, setting base learning rates (κ) to $5e-4$ for CIFAR-10C and CIFAR-100C, and $5e-5$ for ImageNet-C. For balancing parameter sensitivities, we set α to 0.5, 0.9, and 0.5 respectively, with

Method	Gaussian	Shot	Impulse	Defocus	Glass	Motion	Zoom	Snow	Frost	Fog	Brightness	Contrast	Elastic Transform	Pixelate	JPEG	Mean
Source	72.3	65.7	72.9	46.9	54.3	34.8	42.0	25.1	41.3	26.0	9.3	46.7	26.6	58.5	30.3	43.5
BN-1	28.1	26.1	36.3	12.8	35.3	14.2	12.1	17.3	17.4	15.3	8.4	12.6	23.8	19.7	27.3	20.4
Tent Cont.	24.8	20.6	28.6	14.4	31.1	16.5	14.1	19.1	18.6	18.6	12.2	20.3	25.7	20.8	24.9	20.7
CoTTA	24.3	21.3	26.6	11.6	27.6	12.2	10.3	14.8	14.1	12.4	7.5	10.6	18.3	13.4	17.3	16.2
EcoTTA	23.8	18.7	25.7	11.5	29.8	13.3	11.3	15.3	15.0	13.0	7.9	11.3	20.2	15.1	20.5	16.8
AdaContrast	29.1	22.5	30.0	14.0	32.7	14.1	12.0	16.6	14.9	14.4	8.1	10.0	21.9	17.7	20.0	18.5
SFT (cont.)	27.7	24.1	33.8	12.2	33.1	13.1	10.9	15.9	15.6	13.8	7.8	10.8	21.2	16.6	22.9	18.6
DSS	24.1	21.3	25.4	11.7	26.9	12.2	10.5	14.5	14.1	12.5	7.8	10.8	18.0	13.1	17.3	16.0
LAW	24.7	18.9	25.5	12.9	26.7	15.0	11.8	15.1	14.7	15.9	10.1	13.8	19.4	14.7	18.3	17.2
Ours	25.8	18.1	22.7	12.3	25.3	13.1	10.7	13.5	13.1	12.2	8.5	11.8	17.9	12.0	15.4	15.5

Table 1: Mean errors (%) on CIFAR-10C - CTTA mean errors of the 15 corruptions (tasks) at a severity level of 5.

Method	Gaussian	Shot	Impulse	Defocus	Glass	Motion	Zoom	Snow	Frost	Fog	Brightness	Contrast	Elastic Transform	Pixelate	JPEG	Mean
Source	73.0	68	39.4	29.3	54.1	30.8	28.8	39.5	45.8	50.3	29.5	55.1	37.2	74.7	41.2	46.4
BN-1	42.1	40.7	42.7	27.6	41.9	29.7	27.9	34.9	35.0	41.5	26.5	30.3	35.7	32.9	41.2	35.4
Tent Cont.	37.2	35.8	41.7	37.9	51.2	48.3	48.5	58.4	63.7	71.1	70.4	82.3	88.0	88.5	90.4	60.9
CoTTA	40.1	37.7	39.7	26.9	38.0	27.9	26.4	32.8	31.8	40.3	24.7	26.9	32.5	28.3	33.5	32.5
AdaContrast	42.3	36.8	38.6	27.7	40.1	29.1	27.5	32.9	30.7	38.2	25.9	28.3	33.9	33.3	36.2	33.4
SFT (cont.)	40.7	36.3	37.8	25.5	39.0	27.6	25.2	32.2	30.4	37.3	23.7	26.8	32.3	27.6	37.2	32.0
DSS	39.7	36.0	37.2	26.3	35.6	27.5	25.1	31.4	30.0	37.8	24.2	26.0	30.0	26.3	31.1	30.9
LAW	41.0	36.7	38.3	25.6	37.0	27.8	25.2	30.7	30.0	37.3	24.4	27.6	31.2	27.8	34.9	31.7
Ours	37.3	32.5	34.9	26.2	35.3	27.5	24.6	28.8	29.1	34.1	23.5	26.9	31.2	26.6	34.1	30.1

Table 2: Mean errors (%) on CIFAR-100C - CTTA mean errors of the 15 corruptions (tasks) at a severity level of 5.

temperature coefficients T set to 50, 100, and 1000 respectively. We set η to 1, 0.5, and 0.3, and λ to 0.01 throughout. Batch sizes are set to 200, 200, and 64 for each dataset, following CoTTA, and results are only reported for the highest severity level of 5 for each task.

GTTA implementation details: In the standard CTTA setup, each task only receives images with the highest severity. However, in GTTA, following CoTTA, for each task, the severity levels are gradually changed as $\dots \rightarrow 1 \xrightarrow[\text{change}]{\text{task}}$

$1 \rightarrow 2 \rightarrow 3 \rightarrow 4 \rightarrow 5 \rightarrow 4 \rightarrow 3 \rightarrow 2 \rightarrow 1 \xrightarrow[\text{change}]{\text{task}} 1 \rightarrow 2 \dots$. We adhere

to the details specified in the CTTA setting.

Baselines: We compare against several CTTA baselines, including BN Stats Adapt (BN-1) (Schneider et al. 2020), Tent Cont. (Wang et al. 2020), CoTTA (Wang et al. 2022), EcoTTA (Song et al. 2023), AdaContrast (Chen et al. 2022), DSS (Wang et al. 2024), and LAW (Park et al. 2024). We also contrast our work against surgical fine-tuning (Lee et al. 2022). For EcoTTA, we report the results on CIFAR-10C and ImageNet-C only since they do not use ResNeXt-29 (Xie et al. 2017) for CIFAR-100C. Following the findings of (Lee et al. 2022), we continually fine-tune only the first convolutional block of the respective models, denoted as ‘‘SFT (cont.)’’, using an SGD optimizer with fixed learning rates of $1e-3$ for the CIFAR datasets and $5e-4$ for ImageNet-C. For the results of LAW, we reproduce their results strictly following their official implementation¹ with parameters as

¹<https://github.com/junia3/LayerwiseTTA/tree/main>

mentioned in their paper.

CTTA Classification Results

Results on CIFAR-10C and CIFAR-100C: We report the CTTA results in Tables 1 and 2. Our method performs the best across all training setups and baselines for both datasets. We achieve large improvements of 4.9% and 5.2% for CIFAR-10C and 5.3% and 30.8% for CIFAR-100C, over BN-1 and Tent Cont. respectively. Concerning recent works of LAW and DSS, our method improves by 1.7% and 0.5% on CIFAR-10C and 1.6% and 0.8% on CIFAR-100C, respectively. Tent Cont. excels initially but accumulates errors over time, increasing mean error. In CoTTA, the method’s reliance on full model updates renders it computationally expensive and unsuitable for deployment. An interesting observation is that with a drastic reduction in the number of trainable parameters, as in SFT (cont.), the mean errors are better than most CTTA benchmarks, if not the best. LAW uses the uncertain pseudo labels to calculate the domain shift approximated via the FIM. The minor error that is introduced for each batch begins to propagate across all the domains. In addition, the imbalance caused by the ‘‘domain-level’’ FIM and the current batch’s FIM, results in a higher error rate for the initial tasks. In our method, the computation of the model prediction uncertainty to automatically select layers is useful (Eq. 1). This confirms the findings in SFT (Lee et al. 2022) that concentrated adaptation, for image corruptions, in the initial layers suffices.

Results on Imagenet-C: In Table 3, we report the CTTA re-

Method	Gaussian	Shot	Impulse	Defocus	Glass	Motion	Zoom	Snow	Frost	Fog	Brightness	Contrast	Elastic Transform	Pixelate	JPEG	Mean
Source	97.8	97.1	98.2	81.7	89.8	85.2	78.0	83.5	77.1	75.9	41.3	94.5	82.5	79.3	68.6	82.0
BN-1	85.0	83.7	85.0	84.7	84.3	73.7	61.2	66.0	68.2	52.1	34.9	82.7	55.9	51.3	59.8	68.6
Tent Cont.	81.6	74.6	72.7	77.6	73.8	65.5	55.3	61.6	63.0	51.7	38.2	72.1	50.8	47.4	53.3	62.6
CoTTA	84.7	82.1	80.6	81.3	79.0	68.6	57.5	60.3	60.5	48.3	36.6	66.1	47.2	41.2	46.0	62.7
EcoTTA	-	-	-	-	-	-	-	-	-	-	-	-	-	-	-	63.4
AdaContrast	82.9	80.9	78.4	81.4	78.7	72.9	64.0	63.5	64.5	53.5	38.4	66.7	54.6	49.4	53.0	65.5
SFT (cont.)	83.4	79.5	77.2	86.1	82.4	72.2	61.1	63.1	64.7	51.2	35.9	72.9	56.2	46.7	50.2	65.5
DSS	84.6	80.4	78.7	83.9	79.8	74.9	62.9	62.8	62.9	49.7	37.4	71.0	49.5	42.9	48.2	64.6
LAW	81.8	75.0	72.1	77.4	73.2	63.9	54.6	57.9	61.0	50.1	36.3	68.6	49.0	46.2	49.1	61.0
Ours	81.1	73.3	70.8	77.0	71.8	62.3	53.9	56.7	60.8	50.4	36.2	65.9	48.0	45.2	48.0	60.1

Table 3: Mean errors (%) on ImageNet-C - CTTA mean errors of the 15 corruptions (tasks) at a severity level of 5.

sults on the ImageNet-C dataset. As shown, our method outperforms all the previous CTTA baselines and SFT (cont.). We observe an improvement of 0.9% and 4.5% over LAW and DSS respectively. In addition, we achieve 2.6%, 5.4%, and 2.5% improvements over CoTTA, AdaContrast, and Tent Cont., respectively.

Dataset	Source	BN-1	TENT Cont.	CoTTA	AdaContrast	SFT (cont.)	LAW	Ours
CIFAR-10C	24.7	13.7	20.4	10.9	12.1	11.3	10.9	9.5
CIFAR-100C	33.6	29.9	74.8	26.3	33.0	25.3	27.2	26.1
ImageNet-C	58.4	48.3	46.4	38.8	66.3	41.4	40.5	38.5

Table 4: Mean errors (in %) on CIFAR-10C, CIFAR-100C, and ImageNet-C - GTTA mean errors averaged across all severity levels (1→2→3→4→5).

GTTA Classification Results

Results: Here, we present the GTTA results on the benchmark datasets. For each task, the corruption severity of the inputs is gradually changed as discussed earlier. Table 4 reports the mean classification error for GTTA across all severities. We observe that, for all the datasets, our approach outperforms or performs comparably well across all the reported baselines. With most parameters frozen during the adaptation on each batch, our method is more robust and inexpensive than CoTTA, which also demonstrates competitive improvements in the mean classification error.

Ablation Studies and Analysis

Computational efficiency and Catastrophic forgetting

(CF): In our PALM, we first select a subset of layers from the gradient space (Eq. 2) and adapt them while strictly freezing the unselected layers. In Table 5, we report the average % of adapted model parameters per task with respect to the source model, for our method and CoTTA, across the benchmark datasets. Our method is computationally inexpensive and on an average updates 4.34%, 6.65%, and 17.21% of their respective source parameters. This showcases significant computational advantages over CoTTA, which updates 100% of the parameters. With a single

NVIDIA A5000 GPU, PALM incurs a slightly higher adaptation time/batch, due to the two-stage proposed method. For example, on CIFAR-10, PALM runs for 0.8s per batch, whereas SFT (cont.) and LAW take 0.45 s and 0.73 s respectively. Our method alleviates CF by only adapting a small subset of model parameters, ensuring that much of the prior source knowledge is preserved. Quantitatively, the source models achieved zero-shot mean accuracies of 94.03%, 76.06%, and 75.19% on respective datasets. After adaptation, PALM retained source knowledge better, with mean accuracies of 92.29%, 77.46%, and 70.87%, compared to LAW’s 91.67%, 77.69%, and 71.57%. Despite the accuracy decline with more tasks, especially after adaptation on ImageNet-C, PALM matches or outperforms LAW.

Dataset	Ours	CoTTA	Dataset	Ours	LARS	Prodigy	Adafactor
CIFAR-10C	4.34	100	CIFAR-10C	15.5	18.9	20.4	73.8
CIFAR-100C	6.65	100	CIFAR-100C	30.1	34.1	35.5	97.7
ImageNet-C	17.21	100	ImageNet-C	60.1	62.0	68.6	99.2

Table 5: The average % of adapted source parameters/task. Table 6: CTTA mean errors (%) using adaptive LR optimizers vs. ours.

Adaptive LR optimizers vs Ours: Here, we study the effect of directly using adaptive LR optimizers like LARS (You, Gitman, and Ginsburg 2017), Prodigy (Mishchenko and Defazio 2023), and Adafactor (Shazeer and Stern 2018), for CTTA. We report the results in Table 6. The mentioned optimizers do not adjust layer-wise LR based on parameter sensitivity, failing to capture rapid domain shifts and resulting in poorer performance compared to our method.

Analysis of LR importance $i_{j,n}^t$: The prime objective of our work is to adaptively alter the LR of parameters of selected layers based on their sensitivity. In Figure 2, we illustrate how the LR importance $i_{j,n}^t$ (Eq. 7) of WideResNet-28, ResNeXt-29, and ResNet-50, averaged for a task, change during adaptation on their respective datasets. For brevity, we show two domains - glass.blur and snow. We observe that the importance varies across domains and models. Across all the models, we notice that generally, the deeper layers have smaller associated $i_{j,n}^t$, which means that the initial layers are adapted more to the target domain. This result

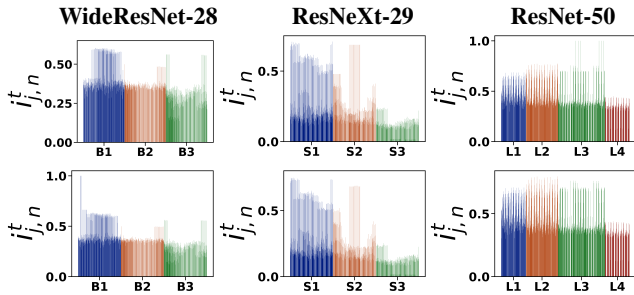


Figure 2: Illustrations of LR importance $i_{j,n}^t$ across different convolutional blocks(B)/stages(S)/layers(L) during CTTA. [Top row] - Variations for the domain “glass_blur” across datasets. [Bottom row] - Variations for the domain “snow”.

Dataset	Pseudo-labels	Ours
CIFAR-10C	17.9	15.5
CIFAR-100C	33.8	30.1
ImageNet-C	68.6	60.1

Table 7: Prediction uncertainty using pseudo-labels vs. ours.

λ	0	0.01	0.05	0.1	0.5	1.0
CIFAR-10C	16.8	15.5	16.4	17.0	17.6	17.9
CIFAR-100C	30.4	30.1	30.5	30.5	30.6	30.7
ImageNet-C	63.9	60.1	60.3	60.4	60.4	60.4

Table 8: Ablation results with varying λ .

completely aligns with the findings of surgical fine-tuning (Lee et al. 2022). In addition to that, we also notice more sparsity in the deeper layers. This further confirms the necessity of freezing parameters automatically selected based on the target domain for adaptation.

Layer importance via pseudo-labels: LAW leverages pseudo-labels to determine layer importance for adaptation. We evaluate the effectiveness of this design for our method by investigating the utility of pseudo-label-based layer importance. We compute the gradients from the log-likelihood as $\nabla_{\theta_{j,n}^t} \log(p(x_k))$ and estimate the sensitivity of the parameters of the chosen layers (Eq. 4-Eq. 6), and alter the LR (Eq. 7). Table 7 reports the mean classification errors for all the datasets. We observe that such gradients are unreliable indicators of prediction uncertainty. The scoring function $\mathcal{Z}_{\theta_{j,n}^t} = \|\nabla_{\theta_{j,n}^t} \mathcal{L}(\theta^t)\|_1$ computed using these gradients carries insufficient information. We achieve improvements of 2.4%, 3.7%, and 8.5% over CIFAR-10C, CIFAR-100C, and ImageNet-C, respectively.

Effectiveness of temperature T : In our method, we compute the KL divergence between the uniform distribution \mathbf{u} and a smoothed classifier’s output logits (Eq. 1), denoted by $\hat{h}(x_k)$. We illustrate the results in Figure 3(a) to study its influence. Ideally, larger values of T push the distributions of the predictions closer to \mathbf{u} (Hinton, Vinyals, and Dean 2015) by spreading the probability among inputs. In CTTA, since we deal with domain shifts with no labels, we argue that higher values of T are useful to capture the uncertainty. So, the KL divergence reduces, indicating more uncertainty in the model and hence, more adaptation. For a systematic temperature selection, we aim to adjust T based on the num-

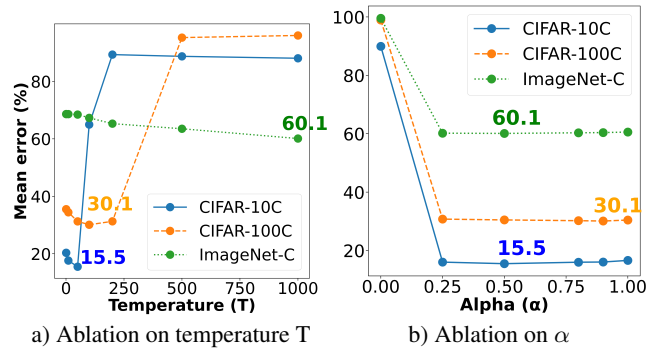


Figure 3: Ablation results on smoothing factor α and temperature T .

ber of adapted parameters. In particular, if the number of adapted parameters increases across batches, T will be increased. For a difficult dataset like ImageNet-C, larger values of T are useful with the error reducing as T increases. For the CIFAR-C datasets, the errors begin to rise for $T \geq 100$ which could be due to large spreads of the distributions.

Contribution of smoothing factor α : A key component of PALM is computing the moving average of sensitivities across data batches, smoothed by α (Eq. 5). Figure 3(b) illustrates the variations of the mean errors, for the benchmark datasets, for varying α . We observe that the “domain-level” sensitivity across past batches of data is indeed useful. For $\alpha = 0$ *i.e.*, when $S_{j,n}^t$ of a selected parameter at timestep t is not considered, the respective datasets’ error rate drastically spikes. For CIFAR-10C, we achieve the best performance when $\alpha = 0.5$ with an improvement of 1.7% over LAW. For CIFAR-100C and ImageNet-C, we see improvements of 1.6% and 0.9% over LAW, at $\alpha = 0.9$ and 0.5 respectively. With higher values of α , the results do not vary too much. Hence, attaining a balance between sensitivities from past domains ($\hat{S}_{j,n}^t$) and current sensitivity ($S_{j,n}^t$) is needed.

Robustness to λ : In Eq. 11, we set $\lambda \in \{0, 0.01, 0.05, 0.1, 0.5, 1.0\}$. Table 8 reports the average classification errors on the benchmark datasets. For $\lambda = 0.01$, we achieve the best results. In addition, we observe that our method is very robust to λ *i.e.*, with subtle variations to differing λ .

Conclusion

In this paper, we propose a novel approach called PALM, for continual test-time adaptation. Our approach automatically decides on the importance of a layer by leveraging information from the gradient space *i.e.*, by backpropagating the KL divergence between a uniform distribution and the softmax outputs. This effectively eliminates the need for pseudo-labels. For the parameters of these layers, selected based on the norm of the gradients, the LR are adjusted based on their sensitivity to domain shift. Extensive experiments are conducted on benchmark datasets to demonstrate the efficacy of our method against different baselines. The results reveal that PALM achieves superior performance and pushes the state-of-the-art on several standard baselines.

Acknowledgments

We thank all the reviewers for their helpful comments and suggestions. This project was supported by a grant from the University of Texas at Dallas, Richardson, TX, USA.

References

- Arnold, E.; Al-Jarrah, O. Y.; Dianati, M.; Fallah, S.; Oxtoby, D.; and Mouzakitis, A. 2019. A survey on 3d object detection methods for autonomous driving applications. *IEEE Transactions on Intelligent Transportation Systems*, 20(10): 3782–3795.
- Chen, D.; Wang, D.; Darrell, T.; and Ebrahimi, S. 2022. Contrastive test-time adaptation. In *Proceedings of the IEEE/CVF Conference on Computer Vision and Pattern Recognition*, 295–305.
- Croce, F.; Andriushchenko, M.; Sehwag, V.; DeBenedetti, E.; Flammarion, N.; Chiang, M.; Mittal, P.; and Hein, M. 2020. Robustbench: a standardized adversarial robustness benchmark. *arXiv preprint arXiv:2010.09670*.
- Döbler, M.; Marsden, R. A.; and Yang, B. 2023. Robust mean teacher for continual and gradual test-time adaptation. In *Proceedings of the IEEE/CVF Conference on Computer Vision and Pattern Recognition*, 7704–7714.
- Gong, T.; Jeong, J.; Kim, T.; Kim, Y.; Shin, J.; and Lee, S.-J. 2022. Robust continual test-time adaptation: Instance-aware bn and prediction-balanced memory. *arXiv preprint arXiv:2208.05117*.
- Guo, Y.; Shi, H.; Kumar, A.; Grauman, K.; Rosing, T.; and Feris, R. 2019. Spottune: transfer learning through adaptive fine-tuning. In *Proceedings of the IEEE/CVF conference on computer vision and pattern recognition*, 4805–4814.
- He, K.; Zhang, X.; Ren, S.; and Sun, J. 2016. Deep residual learning for image recognition. In *Proceedings of the IEEE conference on computer vision and pattern recognition*, 770–778.
- Hendrycks, D.; and Dietterich, T. 2019. Benchmarking neural network robustness to common corruptions and perturbations. *arXiv preprint arXiv:1903.12261*.
- Hinton, G.; Vinyals, O.; and Dean, J. 2015. Distilling the knowledge in a neural network. *arXiv preprint arXiv:1503.02531*.
- Huang, R.; Geng, A.; and Li, Y. 2021. On the importance of gradients for detecting distributional shifts in the wild. *Advances in Neural Information Processing Systems*, 34: 677–689.
- Jain, V.; and Learned-Miller, E. 2011. Online domain adaptation of a pre-trained cascade of classifiers. In *CVPR 2011*, 577–584. IEEE.
- Kirkpatrick, J.; Pascanu, R.; Rabinowitz, N.; Veness, J.; Desjardins, G.; Rusu, A. A.; Milan, K.; Quan, J.; Ramalho, T.; Grabska-Barwinska, A.; et al. 2017. Overcoming catastrophic forgetting in neural networks. *Proceedings of the national academy of sciences*, 114(13): 3521–3526.
- LeCun, Y.; Denker, J.; and Solla, S. 1989. Optimal brain damage. *Advances in neural information processing systems*, 2.
- Lee, N.; Ajanthan, T.; and Torr, P. H. 2018. Snip: Single-shot network pruning based on connection sensitivity. *arXiv preprint arXiv:1810.02340*.
- Lee, Y.; Chen, A. S.; Tajwar, F.; Kumar, A.; Yao, H.; Liang, P.; and Finn, C. 2022. Surgical fine-tuning improves adaptation to distribution shifts. *arXiv preprint arXiv:2210.11466*.
- Liang, C.; Jiang, H.; Zuo, S.; He, P.; Liu, X.; Gao, J.; Chen, W.; and Zhao, T. 2022. No parameters left behind: Sensitivity guided adaptive learning rate for training large transformer models. *arXiv preprint arXiv:2202.02664*.
- Long, M.; Zhu, H.; Wang, J.; and Jordan, M. I. 2016. Unsupervised domain adaptation with residual transfer networks. *Advances in neural information processing systems*, 29.
- Luo, J.-H.; Wu, J.; and Lin, W. 2017. Thinet: A filter level pruning method for deep neural network compression. In *Proceedings of the IEEE international conference on computer vision*, 5058–5066.
- Mishchenko, K.; and Defazio, A. 2023. Prodigy: An expeditiously adaptive parameter-free learner. *arXiv preprint arXiv:2306.06101*.
- Molchanov, P.; Mallya, A.; Tyree, S.; Frosio, I.; and Kautz, J. 2019. Importance estimation for neural network pruning. In *Proceedings of the IEEE/CVF conference on computer vision and pattern recognition*, 11264–11272.
- Molchanov, P.; Tyree, S.; Karras, T.; Aila, T.; and Kautz, J. 2016. Pruning convolutional neural networks for resource efficient inference. *arXiv preprint arXiv:1611.06440*.
- Mozer, M. C.; and Smolensky, P. 1988. Skeletonization: A technique for trimming the fat from a network via relevance assessment. *Advances in neural information processing systems*, 1.
- Niu, S.; Wu, J.; Zhang, Y.; Chen, Y.; Zheng, S.; Zhao, P.; and Tan, M. 2022. Efficient test-time model adaptation without forgetting. In *International conference on machine learning*, 16888–16905. PMLR.
- Park, J.; Kim, J.; Kwon, H.; Yoon, I.; and Sohn, K. 2024. Layer-wise Auto-Weighting for Non-Stationary Test-Time Adaptation. In *Proceedings of the IEEE/CVF Winter Conference on Applications of Computer Vision*, 1414–1423.
- Rasmussen, C.; and Ghahramani, Z. 2000. Occam’s razor. *Advances in neural information processing systems*, 13.
- Ro, Y.; and Choi, J. Y. 2021. Autolr: Layer-wise pruning and auto-tuning of learning rates in fine-tuning of deep networks. In *Proceedings of the AAAI Conference on Artificial Intelligence*, volume 35, 2486–2494.
- Sagun, L.; Evci, U.; Guney, V. U.; Dauphin, Y.; and Bottou, L. 2017. Empirical analysis of the hessian of over-parametrized neural networks. *arXiv preprint arXiv:1706.04454*.
- Schneider, S.; Rusak, E.; Eck, L.; Bringmann, O.; Brendel, W.; and Bethge, M. 2020. Improving robustness against common corruptions by covariate shift adaptation. *Advances in neural information processing systems*, 33: 11539–11551.
- Schwarz, J.; Czarnecki, W.; Luketina, J.; Grabska-Barwinska, A.; Teh, Y. W.; Pascanu, R.; and Hadsell, R.

2018. Progress & compress: A scalable framework for continual learning. In *International conference on machine learning*, 4528–4537. PMLR.
- Sener, O.; Song, H. O.; Saxena, A.; and Savarese, S. 2016. Learning transferrable representations for unsupervised domain adaptation. *Advances in neural information processing systems*, 29.
- Shannon, C. E. 1948. A mathematical theory of communication. *The Bell system technical journal*, 27(3): 379–423.
- Shazeer, N.; and Stern, M. 2018. Adafactor: Adaptive learning rates with sublinear memory cost. In *International Conference on Machine Learning*, 4596–4604. PMLR.
- Song, J.; Lee, J.; Kweon, I. S.; and Choi, S. 2023. EcoTTA: Memory-Efficient Continual Test-time Adaptation via Self-distilled Regularization. In *Proceedings of the IEEE/CVF Conference on Computer Vision and Pattern Recognition*, 11920–11929.
- Sun, Y.; Wang, X.; Liu, Z.; Miller, J.; Efros, A.; and Hardt, M. 2020. Test-time training with self-supervision for generalization under distribution shifts. In *International conference on machine learning*, 9229–9248. PMLR.
- Theis, L.; Korshunova, I.; Tejani, A.; and Huszár, F. 2018. Faster gaze prediction with dense networks and fisher pruning. *arXiv preprint arXiv:1801.05787*.
- Wang, D.; Shelhamer, E.; Liu, S.; Olshausen, B.; and Darrell, T. 2020. Tent: Fully test-time adaptation by entropy minimization. *arXiv preprint arXiv:2006.10726*.
- Wang, Q.; Fink, O.; Van Gool, L.; and Dai, D. 2022. Continual test-time domain adaptation. In *Proceedings of the IEEE/CVF Conference on Computer Vision and Pattern Recognition*, 7201–7211.
- Wang, Y.; Hong, J.; Cheraghian, A.; Rahman, S.; Ahmedt-Aristizabal, D.; Petersson, L.; and Harandi, M. 2024. Continual test-time domain adaptation via dynamic sample selection. In *Proceedings of the IEEE/CVF Winter Conference on Applications of Computer Vision*, 1701–1710.
- Xie, S.; Girshick, R.; Dollár, P.; Tu, Z.; and He, K. 2017. Aggregated residual transformations for deep neural networks. In *Proceedings of the IEEE conference on computer vision and pattern recognition*, 1492–1500.
- Yosinski, J.; Clune, J.; Bengio, Y.; and Lipson, H. 2014. How transferable are features in deep neural networks? *Advances in neural information processing systems*, 27.
- You, Y.; Gitman, I.; and Ginsburg, B. 2017. Large batch training of convolutional networks. *arXiv preprint arXiv:1708.03888*.
- Zagoruyko, S.; and Komodakis, N. 2016. Wide residual networks. *arXiv preprint arXiv:1605.07146*.
- Zeiler, M. D.; and Fergus, R. 2014. Visualizing and understanding convolutional networks. In *Computer Vision—ECCV 2014: 13th European Conference, Zurich, Switzerland, September 6–12, 2014, Proceedings, Part I 13*, 818–833. Springer.
- Zhang, C.; Bengio, S.; and Singer, Y. 2022. Are all layers created equal? *The Journal of Machine Learning Research*, 23(1): 2930–2957.
- Zintgraf, L.; Shiarli, K.; Kurin, V.; Hofmann, K.; and Whiteson, S. 2019. Fast context adaptation via meta-learning. In *International Conference on Machine Learning*, 7693–7702. PMLR.